Microsystem Technologies (2019) 25:4097–4110
https://doi.org/10.1007/s00542-019-04351-0

TECHNICAL PAPER

Nonlinear free vibration analysis of pre-actuated isotropic piezoelectric cantilever Nano-beams

Hossein Vaghefpour[1] · Hadi Arvin[1]

Received: 7 December 2018 / Accepted: 8 February 2019 / Published online: 22 February 2019

Abstract
In this paper, nonlinear free vibration analysis of pre-actuated clamped-free isotropic piezoelectric Euler-Bernoulli nanobeams is discussed. The governing equations of motion are derived on the basis of size-dependent piezoelectricity theory. A more accurate model is developed for the large amplitude vibration analysis of piezoelectric cantliver nanobeams by the consideration of a higher order curvature-displacement relation. In this case, a nonlinear equation of motion is derived. Accordingly, the hardening or softening treatment dependency on the flexoelectric constant and the length scale parameter is examined for the considered nanocantilever. The assumed nano-beam is actuated by a constant voltage. The nonlinear free vibration analysis of pre-actuated nano-beam about the pre-static deformation is examined by Lindstedt-Poincare technique which is applied on the discretized equations of motion. A closed form relation is extracted for the nonlinear natural frequency and the corresponding effective nonlinearity. Some numerical analysis has been performed to peruse the effects of applied voltage, the length scale parameter and flexoelectric coefficient on the static deflection, the nonlinear natural frequencies and the associated effective nonlinearities. The outcomes demonstrate occurrence of very interesting phenomena in the combination of the various magnitudes of the length scale parameter and the flexoelectric coefficient.

1 Introduction

Micro and nano electromechanical systems (MEMS and NEMS) have great potential applications in the field of mechanical, civil, aerospace and other engineering areas (Ebrahimi and Barati 2018). On the other hand, piezoelectric beams and plates have been widely used in MEMS and NEMS such as those in sensors (Asif et al. 2017) and actuators (Ebrahimi and Barati 2018). Piezoelectric cantilever beams as a kind of piezoelectric actuators are used in MEMS and NEMS because of their simplicity and reliability (Yang et al. 2015). Piezoelectric cantilever nanobeams are often implemented in the form of laminated nanobeams and nanoplates, such as unimorph, bimorph, multimorph, etc (Lim et al. 2006; Lazarus et al. 2012). The intrinsic electromechanical coupling, known as direct and inverse piezoelectric effects, makes piezoelectric materials useful for a variety of electromechanical systems. Therefore, nanodevices with piezoelectric elements are handy for a variety of electromechanical systems which are implemented for sensing vibration and for noise control (Sumali et al. 2001; Casadei et al. 2010), energy harvesting (Haq 2019) and sensor networks (Hao and Liao 2010). Because of their novel properties, nanomaterials have a great chance to be employed in various types of nanodevices, such as nanoresonators (Tanner et al. 2007), field effect transistors (Fei et al. 2009) and light emitting diodes (He et al. 2007). Hence, study on the piezoelectric nanobeams has great advantages. In recent decades, researchers have implemented higher-order continuum theories to derive the governing equations of nanostructures.

Thanks to the recent developments in nanomechanics, size-dependent electromechanical theories with coupled mechanical and electrical effects are also developed such as size-dependent piezoelectricity (Barati 2017). The macro scale piezoelectricity theory states the relation between the electric polarization and uniform strain in non-centrosymmetric materials (Cady 1964). However, some researchers have illustrated the size-effect in piezoelectric properties and linear electromechanical coupling in isotropic dielectrics (Ebnali Samani and Tadi Beni 2018;

✉ Hadi Arvin
hadi.arvin@sku.ac.ir

[1] Faculty of Engineering, Shahrekord University, Shahrekord, Iran

Baskaran 2011). Wang et al. (2014) developed a size-dependent piezoelectricity theory based on the couple stress theory. In the proposed theory, the dielectric polarization depends not only on the strain tensor but also on the curvature tensor (Zeng et al. 2017). Hence, it can be deduced that the flexoelectric effect is universally present in all dielectrics (Hadjesfandiari 2013). In this respect, other theories were also developed, although they exhibit limitations due to the consideration of the inconsistent second order deformation gradients or dropping off the couple stress effect. Hadjesfandiari and Dargush (2011) recently proposed the size-dependent piezoelectricity theory. They expressed the behavior of continuous materials in the small scales on the basis of the electromechanical formulation. In this theory, the size-dependent piezoelectricity or flexoelectric effect is derived depending on the mean curvature tensor. A number of researchers have examined the piezoelectric nanobeams by employing the size-dependent theories. They have studied on the mechanical and electrical equations of the nanobeams (Maranganti 2006). Tadi Beni (2017) derived the piezoelectric nanobeam formulation in general case by using the size-dependent piezoelectricity theory.

The piezoelectric nanobeams with an AC or DC applied voltage is often implemented in NEMS. The DC applied voltage enforces the nanobeam to a new equilibrium position (static deflection) (Younis and Nayfeh 2003). The static deflection and the vibration of microbeams with DC electrostatic actuation or combined AC-DC electrostatic actuation have been studied in Rasekh and Khadem (2011), Kim et al. (2012). On the other hand, piezoelectric nanobeams can utilize as sensors, due to their unique properties, to detect with great accuracy physical quantities such as, viruses, bacteria, and cells (Park et al. 2010; Yang et al. 2011). Wu et al. (2001) implemented the static deflection to mass detection of chemical and biological elements. An alternate and more attractive approach to examine the sensitivity to mass detection is forcing a piezoelectric cantilever nanobeam to oscillate around one of its natural frequencies. The sensitivity analysis of the NEMS was examined in Lavrik and Datskos (2003), Raiteri et al. (2001) while an NEMS device operate in the dynamic mode about one of its natural frequencies.

Cantilever beams are used widely as elements in resonant sensors. Number of studies have evaluated the frequency shifts in cantilever beams. Dohn et al. (2005) evaluated the sensitivity of a cantilever beam as a mass detective sensor to the location of the added mass along the beam span. They concluded that maximum sensitivity happens at the beam tip point. They also deduced that the sensitivity has a mutual relation with the mode number.

According to the literature review, most of the previous researcher have focused on the vibration, buckling and the static deflection of piezoelectric nanobeams. On the other hand, the frequency analysis has been investigated only during the electrostatic actuation. There are some advantages in employing piezoelectric nanobeams instead of electrostatically actuated nanobeams. The electrostatically actuated systems have at least two separated parts: beam and electrode. These systems may also undergo a destructive pull-in phenomenon. So, it is useful to replace the electrostatic actuators with a piezoelectric nanobeam. Therefore it seems necessary to study on the nonlinear frequency analysis of piezoelectric nanobeams. The novelty of this paper is the investigation on the nonlinear frequency of piezoelectric nanobeams with higher order curvature displacement relation under applied DC voltage.

As it was mentioned earlier, one of the important technique for the investigation on the sensitivity of the sensors to mass detection is enforcing a piezoelectric cantilever nanobeam to vibrate around one of its natural frequencies. So, the exact computation of the natural frequencies is very important. On the other hand, the nano cantilevers experience large deformations. In this case, being familiar with the nonlinear treatment of the nano cantilever which it will show a hardening or softening behavior in the large amplitude vibration with the variation in the structure parameters will be really essential and constructive. It is worth to mention that in the available formulations by the consideration of the von-Karman strain displacement relation, a linear governing equation of motion is accessible for a cantilever nanobeam. Thereafter, accordingly, the nonlinear treatment cannot be examined. Hence, in this paper a higher order nonlinear size-dependent formulation for a cantilever piezoelectric Euler-Bernoulli nanobeam which is subjected to an applied voltage is developed by the implementation of the Hamilton's principle based on the nonclassical continuum mechanics. The contributions of this paper are as follows; For achieving a higher order formulation, a third-order relation is considered for describing the curvature in terms of the axial and transverse deformations. The linear and nonlinear vibration of a piezoelectric nanobeam is extracted about the pre-static deflection. The Galerkin projection technique is implemented to discretize the governing PDEs to ODEs. The nonlinear pre-static deflection problem is carried out employing the Galerkin discretization approach. The achieved nonlinear ODE is solved employing the Lindstedt-Poincare approach. After verification of the outcomes, some numerical analysis is conducted in details to investigate the effects of applied voltage, length scale and flexoelectric coefficient on the static deflection, linear natural frequencies, the effective nonlinearity coefficient and the nonlinear natural frequencies. The outcomes illustrate a very interesting phenomena by simultaneous changes in the flexoelectric constant and the material length scale parameter.

2 Governing equations

A cantilever nanobeam made of isotropic piezoelectric material which is subjected to a DC voltage, V_0, is depicted in Fig. 1. The nano-beam width, length, and thickness are, respectively, b, L and h.

The strain energy of a linear isotropic elastic piezoelectric nano-structure, which occupies volume $\mathcal{V}$, employing the size-dependent piezoelectricity theory read as Hadjesfandiari (2013):

$$U = \frac{1}{2}\int_{\mathcal{V}} \left(\sigma_{ji}e_{ij} + \mu_{ji}\kappa_{ij} - D_i E_i\right) dV \tag{1}$$

where $\sigma_{ji}, e_{ij}, \mu_{ji}$ and κ_{ij}, respectively, represent the classical stress tensor, strain tensor, couple-stress tensor, and curvature tensor. D_i and E_i, respectively, stand for the electric displacement vector and the electric field vector. For an elastic isotropic piezoelectric nano-structure, the size-dependent constitutive relations are expressed as Hadjesfandiari (2013):

$$\begin{aligned} \sigma_{ji} &= \lambda e_{kk}\delta_{ij} + 2\mu e_{ij} + 2\mu l^2 \nabla^2 \omega_{ji}, \\ \mu_{ji} &= \epsilon_{ijk}\mu_k, \\ \kappa_{ij} &= \frac{1}{2}(\omega_{i,j} - \omega_{j,i}), \\ D_i &= \varepsilon E_i + 4f\kappa_i \end{aligned} \tag{2}$$

in which μ_i, ω_i and κ_i are defined, respectively, as Hadjesfandiari (2013):

$$\begin{aligned} \mu_i &= -8\mu l^2 \kappa_i + 2fE_i, \\ \omega_i &= \frac{1}{2}\epsilon_{ijk}u_{k,j}, \\ \kappa_i &= \frac{1}{2}\epsilon_{ijk}\kappa_{ij} \end{aligned}$$

where λ and μ are Lame's constants, and l, f, and ε are the size effect parameter, the so-called flexoelectric coefficient, and the dielectric constant (electric permittivity), respectively.

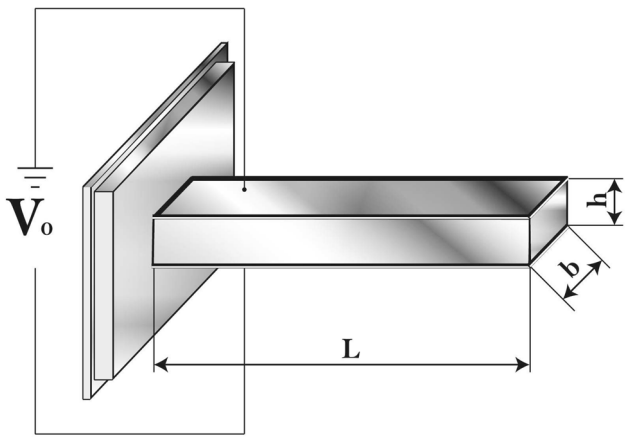

Fig. 1 Schema of an isotropic piezoelectric nano-beam

The electric field vector is the negative gradient of the total potential function (Asif et al. 2017):

$$E_i = -\Phi_{,i} \tag{3}$$

The von-Karman strain-displacement relation for elongation and the third-order relation for curvature in terms of axial and transverse deformations are employed as Lacarbonara (2013):

$$\epsilon = u_{,x} + \frac{1}{2}w_{,x}^2 \tag{4}$$

$$\rho^{(3)} = w_{,xx} - (u_{,x}w_{,x})_{,x} - w_{,x}^2 w_{,xx} \tag{5}$$

in which $()_{,x} \equiv \frac{\partial()}{\partial x}$, $w(x, t)$ is the transverse displacement and $u(x, t)$ is the longitudinal displacement, respectively, along the z and x axes.

The strain field along the thickness is expressed by Lacarbonara (2013):

$$e = \epsilon - z\rho^{(3)} \tag{6}$$

According to Eq. 4, the inextensibility condition yields in:

$$u_{,x} = -\frac{1}{2}w_{,x}^2 \tag{7}$$

Substitution of Eq. 7 into Eq. 5 results in:

$$\rho^{(3)} = w_{,xx} + \frac{1}{2}w_{,x}^2 w_{,xx} \tag{8}$$

By substituting Eq. 8 into Eq. 6, the only non-zero component of the nonlinear strain field read as:

$$e_{11} = -zw_{,xx} - \frac{1}{2}zw_{,x}^2 w_{,xx} \tag{9}$$

By assuming the displacement field for the Euler-Bernoulli beam model as $u_1(x, z, t) = u(x, t) - zw_{,x}(x, t)$, $u_2(x, z, t) = 0$ and $u_3(x, z, t) = w(x, t)$, the kinetic energy of the nano-beam can be expressed by:

$$T = \frac{1}{2}\int_{\mathcal{V}} \rho\left(u_{1,t}^2 + u_{2,t}^2 + u_{3,t}^2\right) dV \tag{10}$$

in which ρ is the mass density of the piezoelectric material.

The Hamilton's principle is employed to extract the governing equations of motion and the corresponding boundary conditions as:

$$\int_{t_0}^{t_1} (\delta T - \delta U)\mathrm{d}t = 0 \tag{11}$$

in which $\int_{t_0}^{t_1}(\delta T)\mathrm{d}t$ is simplified to:

$$\int_{t_0}^{t_1}(\delta T)\mathrm{d}t=\int_{t_0}^{t_1}\left\{-\int_0^L(F_{11}w_{,tt}-H_{11}w_{,ttxx})\delta w dx\right\}dt - \int_{t_0}^{t_1}H_{11}w_{,ttx}\delta w\big|_0^L \tag{12}$$

where $(F_{11},H_{11})=\int_{-b/2}^{b/2}\int_{-h/2}^{h/2}\rho(1,z^2)dydz$ and $\int_{t_0}^{t_1}(\delta U)\mathrm{d}t$ is expressed in Appendix 1.

Hence, the following mechanical and electrical governing equations are obtained:

$$\delta w:(\lambda+2\mu)I\Big(w_{,xxxx}+\left[w_{,x}(w_{,x}w_{,xx})_{,x}\right]_{,x}\Big)+A_{11}w_{,xxxx} - 2(E_{11})_{,xx}+F_{11}w_{,tt}-H_{11}w_{,ttxx}=0 \tag{13}$$

$$\delta\Phi:\quad \epsilon(\Phi_{,xx}+\Phi_{,zz})+2f_{,z}w_{,xx}=\rho_e \tag{14}$$

By neglecting the rotary inertia effect, i.e. H_{11}, and assuming no dielectric charge density in the volume, i.e. $\rho_e=0$, equations of motion, i.e. Eqs. 13 and 14, and the associated mechanical and electrical boundary conditions for a cantilever piezoelectric nanobeam, respectively, reshuffle to:

$$((\lambda+2\mu)I+A_{11})w_{,xxxx}+(\lambda+2\mu)I[w_{,x}(w_{,x}w_{,xx})_{,x}]_{,x} - 2(E_{11})_{,xx}+F_{11}w_{,tt}=0 \tag{15}$$

$$\epsilon(\Phi_{,xx}+\Phi_{,zz})+2f_{,z}w_{,xx}=0 \tag{16}$$

and

$$\Big[((\lambda+2\mu)I+A_{11})w_{,xxx}+(\lambda+2\mu)Iw_{,x}(w_{,x}w_{,xx})_{,x}-2(E_{11})_{,x}\Big]\Big|_0^L=0 \quad \text{or} \quad \delta w|_0^L=0 \tag{17}$$

$$\left[(((\lambda+2\mu)I+A_{11})w_{,xx}+(\lambda+2\mu)Iw_{,x}^2w_{,xx}-2(E_{11})\right]\Big|_0^L=0 \quad \text{or} \quad \delta(w_{,x})|_0^L=0 \tag{18}$$

$$\int_A(\Phi_{,x})dA=0 \quad \text{or} \quad \delta\Phi\Big|_0^L=0 \qquad \int_A[\Phi_{,z}+2f(w_{,xx})]dA=0 \quad \text{or} \quad \delta\Phi\Big|_{-\frac{h}{2}}^{\frac{h}{2}}=0 \tag{19}$$

In this paper, by considering the reverse effect for the piezoelectric nano-beam, the electric potential filed, i.e. Φ, is assumed as Komijani et al. (2014):

$$\Phi(x,z,t)=\cos(\beta z)\Phi(x,t)+\frac{V_0(t)}{h}z \tag{20}$$

where $\beta=\frac{\pi}{h}$ and V_0 denotes the external electric voltage applied to the electrodes of the nano-beam.

By substitution of Eq. 20, into Eq. 3 the electric field vector components read as:

$$\Phi_{,x}(x,z,t)=\cos(\beta z)\Phi_{,x}(x,t) \qquad \Phi_{,z}(x,z,t)=-\beta\sin(\beta z)\Phi(x,t)+\frac{V_0(t)}{h} \tag{21}$$

According to Appendix 1 by assuming f to be a constant, $E_{11}=bfV_0$ and hence $(E_{11})_{,xx}=0$. Thereupon the mechanical equations of motion and the associated boundary conditions reshuffle to:

$$((\lambda+2\mu)I+A_{11})w_{,xxxx}+(\lambda+2\mu)I[w_{,x}(w_{,x}w_{,xx})_{,x}]_{,x} + F_{11}w_{,tt}=0 \tag{22}$$

and

$$\delta w|_0=0 \quad \text{and} \quad ((\lambda+2\mu)I+A_{11})w_{,xxx}+(\lambda+2\mu)I(w_{,x}^2w_{,xxx}+w_{,x}w_{,xx}^2)\Big|^L=0 \quad \delta(w_{,x})\big|_0=0 \quad \text{and} \quad \Big[((\lambda+2\mu)I+A_{11})w_{,xx}+(\lambda+2\mu)Iw_{,x}^2w_{,xx}-2bfV_0(t)\Big]\Big|^L=0 \tag{23}$$

For the sake of simplicity and generality, the following nondimensional parameters are introduced:

$$\overline{w}=\frac{w}{L} \quad \overline{x}=\frac{x}{L} \quad \tau=t\sqrt{\frac{(\lambda+2\mu)I}{\rho AL^4}} \tag{24}$$

Following the nondimensionalization procedure and after elimination of $\overline{(\cdot)}$ sign for the sake of brevity, the dimensionless form of the transverse equation of motion and the related boundary conditions can be expressed, respectively, as:

$$w_{,\tau\tau}+L_sw_{,xxxx}=-\left(w_x^2w_{xxx}+w_xw_{xx}^2\right)_x \tag{25}$$

and

$$\delta w|_0=0 \quad \text{and} \quad L_sw_{,xxx}+w_{,x}^2w_{,xxx}+w_{,x}w_{,xx}^2\Big|^1=0 \quad \delta(w_{,x})\big|_0=0 \quad \text{and} \quad \left[L_sw_{,xx}+w_{,x}^2w_{,xx}-\left(\frac{2bL^2f}{(\lambda+2\mu)Ih}\right)V_0(t)\right]\Big|^1=0 \tag{26}$$

where $L_s=(1+\frac{A_{11}}{(\lambda+2\mu)I})$

3 Solution methodology

3.1 Nonlinear static and dynamic equations of motion

The proposed nonlinear solutions for the static deflection and the free vibration analysis are presented in this section. At first, the total transverse deflection, i,e, $w(x, t)$, is considered as a combination of a static deflection induced by the applied voltage, i,e, $w^s(x)$, and a dynamic deformation, i.e. $w^d(x,t)$, about the assumed static deflection as Arvin (2017):

$$w(x,t) = w^d(x,t) + w^s(x) \tag{27}$$

After substitution of Eq. 27 into equation of motion, i.e. Eq. 25, and the corresponding boundary conditions, i.e. Eq. 26, and by elimination of time-varying terms the following equation and the boundary condition for static deflection is achieved:

$$L_s w^s_{,xxxx} + \left(w^{s2}_{,x} w^s_{,xxx} + w^s_{,x} w^{s2}_{,xx}\right)_{,x} = 0 \tag{28}$$

$$\delta w^s|_0 = 0 \quad \text{and} \quad L_s w^s_{,xxx} + w^{s2}_{,x} w^s_{,xxx} + w^s_{,x} w^{s2}_{,xx}\Big|^1 = 0$$
$$\delta(w^s_{,x})\Big|_0 = 0 \quad \text{and}$$
$$\left[L_s w^s_{,xx} + w^{s2}_{,x} w^s_{,xx} - \left(\frac{2bL^2 f}{(\lambda+2\mu)Ih}\right)V_0\right]\Big|^1 = 0 \tag{29}$$

The numerical solution such as *bvp*4*c* which is a MATLAB subroutine (for more details see Arvin (2018) and Arvin (2017)) as well as semi-analytical solution such as Galerkin method can be implemented to achieve the static deflection. In this paper, the Galerkin technique is employed.

Accordingly after elimination of d superscript, due to brevity, one can obtain the nonlinear dynamic equations about the pre-static deformation as:

$$\begin{aligned} &w_{,\tau\tau} + L_s w_{,xxxx} + w^{s2}_{,x} w_{,xxxx} + w^s_{,xxxx} w^2_{,x} + w^2_{,x} w_{,xxxx} \\ &+ 2w^s_{,x} w^s_{,xxxx} w_{,x} + 2w^s_{,x} w_{,xxxx} w_{,x} + 4(w^s_{,x} w^s_{,xx} w_{,xxx} \\ &+ w^s_{,x} w^s_{,xxx} w_{,xx} + w^s_{,x} w_{,xxx} w_{,xx} + w^s_{,xx} w^s_{,xxx} w_{,x} + w^s_{,xx} w_{,xxx} w_{,x} \\ &+ w^s_{,xxx} w_{,xx} w_{,x} + w_{,xxx} w_{,xx} w_{,x}) + 3w^{s2}_{,xx} w_{,xx} + 3w^{s2}_{,xx} w^2_{,xx} + w^3_{,xx} \end{aligned} \tag{30}$$

3.1.1 Galerkin projection procedure

The Galerkin projection approach is employed to discretize the nonlinear dynamic equations of motion. One can approximate the nonlinear vibration of the piezoelectric nanobeam as Younis and Nayfeh (2003):

$$w = \sum_{i=1}^{n} \psi_i(x) q_i(t) \tag{31}$$

where the $q_i(t)$ is the ith generalized displacement coordinate and $\psi_i(x)$ denotes the ith linear normal mode of a clamped-free isotropic beam given by Nayfeh and Nayfeh (1993):

$$\begin{aligned} \psi_i(x) &= \cosh(r_i x) - \cos(r_i x) \\ &+ \frac{\cos(r_i) + \cosh(r_i)}{\sin(r_i) + \sinh(r_i)}(\sin(r_i x) - \sinh(r_i x)) \end{aligned} \tag{32}$$

where r_i is the ith root of the characteristic equation for clamped-free beams given by $\cos(r)\cosh(r) = -1$ (Nayfeh and Nayfeh 1993).

Substitution of Eq. 31 into the nonlinear transverse equation of motion, i.e. Eq. 30 and applying the Galerkin projection approach leads to the reduced order model of the equation of motion for the motion of the kth mode as:

$$\begin{aligned} &\ddot{q}_k(t) + \alpha_{3,k} q_k(t)^3 + \alpha_{2,k} q_k^2(t) + \alpha_{1,k} q_k(t) = 0 \\ &q_k(0) = a_0 \quad \dot{q}_k(0) = 0 \end{aligned} \tag{33}$$

where $\alpha_{3,k}$, $\alpha_{2,k}$ and $\alpha_{1,k}$ are given, respectively, by:

$$\begin{aligned} \alpha_{3,k} &= \xi_{1,k} + \xi_{2,k} + 4\xi_{3,k}, \\ \alpha_{2,k} &= 2\xi_{4,k} + 4\xi_{5,k} + 4\xi_{6,k} + 4\xi_{7,k} + 3\xi_{8,k} + \xi_{9,k}, \\ \alpha_{1,k} &= 2\xi_{10,k} + L_s\xi_{11,k} + 4\xi_{12,k} + 4\xi_{13,k} \\ &\quad + 4\xi_{14,k} + \xi_{15,k} + 3\xi_{16,k}, \end{aligned}$$

in which $\xi_{1,k}$ to $\xi_{16,k}$ relations are represented in Appendix 2.

3.1.2 Lindstedt-Poincare technique

The Lindstedt-Poincare method is employed to develop the nonlinear free vibration solution for the discretized equation of motion, i.e. Eq. 30. Therefore, the generalized coordinate is considered as $q_k(t,\epsilon) = \epsilon x_1(\tau) + \epsilon^2 x_2(\tau) + \epsilon^3 x_3(\tau)$ where ϵ is a bookkeeping parameter which is used in the perturbation techniques for ordering process of variables and $\tau = \omega_k^{NL}(\epsilon)t$. ω_k^{NL} is the kth nonlinear frequency which is given by $\omega_k^{NL}(\epsilon) = \omega_k + \epsilon\omega_{1,k} + \epsilon^2\omega_{2,k} + \epsilon^3\omega_{3,k}$ (see Barari et al. 2011) in which ω_k is the kth linear natural frequency and $\omega_{i,k}$'s are defined during the solution. By substituting the assumed generalized coordinate in Eq. 33, one can obtain:

$$\begin{aligned} &(\omega_k + \epsilon\omega_{1,k} + \epsilon^2\omega_{2,k})^2 \frac{d^2}{d\tau^2}(\epsilon x_1 + \epsilon^2 x_2 + \epsilon^3 x_3) \\ &+ \alpha_{1,k}(\epsilon x_1 + \epsilon^2 x_2 + \epsilon^3 x_3)^1 + \alpha_{2,k}(\epsilon x_1 + \epsilon^2 x_2 + \epsilon^3 x_3)^2 \\ &+ \alpha_{3,k}(\epsilon x_1 + \epsilon^2 x_2 + \epsilon^3 x_3)^3 = 0 \end{aligned} \tag{34}$$

Following some simplifications, by equating the coefficients of the same power of ϵ and recalling from Eq. 33 that $\omega_k^2 = \alpha_{1,k}$ the ordered equations are achieved as: O (ϵ^1) :

$$\omega_k{}^2\frac{d^2x_1}{d\tau^2}+\omega_k{}^2x_1=0,\quad x_1(0)=a_k=\frac{a_0}{\epsilon}\quad \dot{x_1}(0)=0 \tag{35}$$

$$\mathrm{O}\ (\epsilon^2):$$

$$\omega_k{}^2\frac{d^2x_2}{d\tau^2}+\omega_k{}^2x_2=-\left(2\omega_k\omega_{1,k}\frac{d^2x_1}{d\tau^2}+\alpha_{2,k}x_1^2\right)\quad x_2(0)=0\quad \dot{x_2}(0)=0 \tag{36}$$

$$\mathrm{O}\ (\epsilon^3):$$

$$\omega_k{}^2\frac{d^2x_3}{d\tau^2}+\omega_k{}^2x_3=-\left(2\omega_k\omega_{1,k}\frac{d^2x_2}{d\tau^2}+2\alpha_{2,k}x_1x_2+\omega_{1,k}^2\frac{d^2x_1}{d\tau^2}+2\omega_k\omega_{2,k}\frac{d^2x_1}{d\tau^2}+\alpha_{3,k}x_1^3\right)\quad x_3(0)=0\quad \dot{x_3}(0)=0 \tag{37}$$

The general solution of the first order equation, i.e. Eq. 35, takes the following form:

$$x_1=a_k\cos\phi_k \tag{38}$$

where $\phi_k=\tau+\beta_{k,0}$ in which a_k and $\beta_{k,0}$ are constants and are evaluated from the initial conditions.

Substitution of first order solution, i.e. Eq. 38, into Eq. 36 reshuffles the second order equation as:

$$\omega_k{}^2\frac{d^2x_2}{d\tau^2}+\omega_k{}^2x_2=2\omega_k\omega_{1,k}a_k\cos\phi_k-\frac{1}{2}\alpha_{2,k}a_k^2(1+\cos 2\phi_k) \tag{39}$$

Following the common procedure of perturbation methods, the elimination of the secular term, requires $\omega_{1,k}\equiv 0$, thereupon:

$$x_2=-\frac{\alpha_{2,k}a_k^2}{2\omega_k{}^2}\left(1-\frac{1}{3}\cos 2\phi_k\right) \tag{40}$$

By substituting the firs order and second order solution for x_1 and x_2 in Eq. 37 and recalling that $(\omega_{1,k}=0)$ one can obtain:

$$\omega_k{}^2\frac{d^2x_3}{d\tau^2}+\omega_k{}^2x_3=2\left(\omega_k\omega_{2,k}a_k-\frac{3}{8}\alpha_{3,k}a_k^3+\frac{5}{12}\frac{\alpha_{2,k}^2a_k^3}{\omega_k{}^2}\right)\cos\phi_k-\frac{1}{4}\left(\frac{2\alpha_{2,k}^2}{3\omega_k{}^2}+\alpha_{3,k}\right)a_k^3\cos 3\phi_k \tag{41}$$

Accordingly the elimination of the secular term from Eq. 41, releases $\omega_{2,k}$ as:

$$\omega_{2,k}=\frac{(9\alpha_{3,k}\omega_k{}^2-10\alpha_{2,k}^2)a_k^2}{24\omega_k{}^3} \tag{42}$$

After the elimination of the secular term from the third-order equation, i.e. Eq. 41, the corresponding solution read as:

$$x_3=\frac{1}{32}\left(\frac{2\alpha_{2,k}^2}{3\omega_k{}^4}+\frac{\alpha_{3,k}}{\omega_k{}^2}\right)a_k^3\cos 3\phi_k \tag{43}$$

The substitution of the first, second and third order solutions, respectively, from Eqs. 38, 40 and 43 into the expanded from of x, i.e. $x=\epsilon x_1+\epsilon^2x_x+\epsilon^3x_3$, the nonlinear solution of Eq. 33 is achieved:

$$q_k=a_0\cos(\omega_k^{NL}t+\beta_{k,0})-\frac{a_0^2\alpha_{2,k}}{2\alpha_{1,k}}\left(1-\frac{1}{3}\cos\left[2(\omega_k^{NL}t+\beta_{k,0})\right]\right)+\frac{1}{32}\left(\frac{2\alpha_{2,k}^2}{3\omega_k{}^4}+\frac{\alpha_{3,k}}{\omega_k{}^2}\right)a_0^3\cos\left[3(\omega_k^{NL}t+\beta_{k,0})\right]+O(\epsilon^4) \tag{44}$$

where

$$\omega_k^{NL}=\omega_k+\frac{1}{4}\Gamma_ka_k^2+O(\epsilon^3) \tag{45}$$

in which Γ_k is the kth effective nonlinearity coefficient which is denoted by:

$$\Gamma_k=\frac{(9\alpha_{3,k}\omega_k{}^2-10\alpha_{2,k}^2)}{6\omega_k{}^3}.$$

4 Numerical results and discussion

As it is known, flexoelectricity effect plays a significant role just at nano-scales. Hence, for more illustration, in this paper, a cantilever piezoelectric nanobeam (CPNB) is

Table 1 The geometrical and material data of the assumed piezoelectric nanobeam (Tadi Beni 2017)

Parameter	Description	Value (unit)
L	Beam length	500 (nm)
b	Beam width	10 (nm)
h	Beam thickness	15 (nm)
l	Scale factor	0.2 h
f	Flexoelectric coefficient	$5e^{-12}$ (C/m)
μ	Lame constant	42.9 (GPa)
λ	Lame constant	45.2 (GPa)

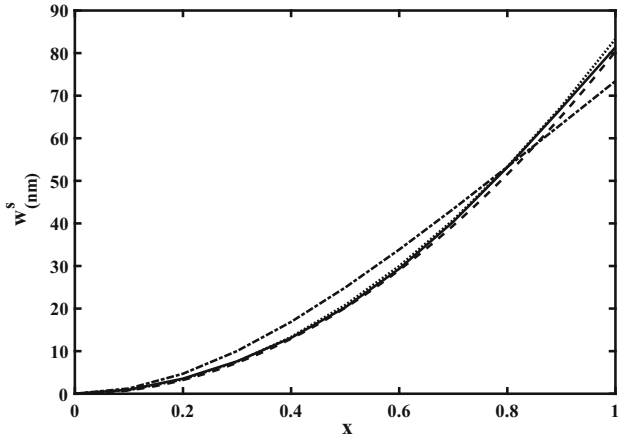

Fig. 2 The current non-linear static deflection achieved by 1-mode Galerkin technique (dotted-dashed-lines), 3-mode Galerkin technique (solid-lines), and the *bvp4c*-subroutine (dashed-lines) versus the corresponding linear analytical results of Tadi Beni (2016) (dotted-lines): ($V_0 = 4000\,v$)

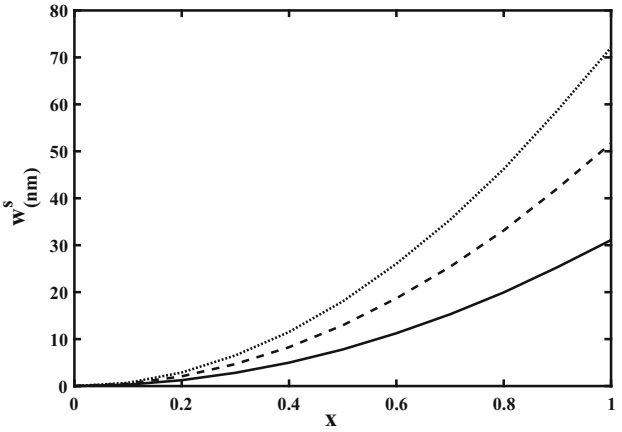

Fig. 3 The nonlinear static deflection of the CPNB for different applied voltages: $V_0 = 1500$ v, solid-lines, $V_0 = 2500$ v, dashed-lines, and $V_0 = 3500$ v, dotted-lines

considered for analysis which is made of $BaTiO_3$. The corresponding geometrical and material data is listed in Table 1. Henceforth, all the employed parameters are same as Table 1 unless new data are prescribed.

To verify the current results, the obtained Galerkin outcomes for the static deflection due to a constant applied voltage are compared with the available linear analytical results which is accessible in Tadi Beni (2016) and the current *bvp4c* results. The comparison is depicted in Fig. 2 for $V_0 = 4000$ v by the consideration of 1 and 3 linear normal modes in Galerkin projection. A very good agreement is clear between the current 3-mode Galerkin projection, the *bvp4c* method and the analytical results. Because the Galerkin approach is very handy in the implementation hence, hereafter 3-mode Galerkin technique is employed for the static deflection computations.

Another verification is confirmed in calculation of linear natural frequency in comparison with Arvin (2018). The considered beam is a rotating micro cantilever beam which is made of epoxy with the mass density, Young modulus, Poisson coefficient and the material length scale parameter, respectively, equal to $\rho = 1220\,\mathrm{kg/m^3}$, $E = 1.4$ GPa, $v = 0.3$ and $l = 17.6\,\mu$m. The slenderness ratio, i.e. $S = L\sqrt{\frac{A}{I}}$, and height to material scale parameter, i.e. $\upsilon = \frac{h}{l}$, are given, respectively, as $S = 30$ and $\upsilon = 1$. In slenderness ratio, L, A and I are, respectively, the beam length, the beam cross-section area and the beam are moment of inertia about y-axis (see Fig. 1). As the considered microbeam is a rotating beam the dimensionless rotation speed is considered as $\lambda_R = 0$ in Fig. 9 of Arvin (2018). The compared results for the first two linear natural frequencies are prepared in Table 2. The results show a very good agreement. It should be noted that in Arvin (2018) the rotary inertia influences are taken into account and hence, the neglecting of rotary inertia here seems reasonable.

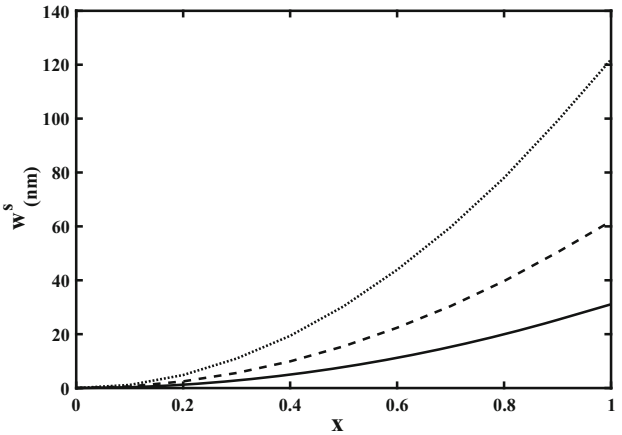

Fig. 4 The effect of the flexoelectric coefficient ($f = 5\,\mathrm{pC/m}$, solid-lines, $f = 10\,\mathrm{pC/m}$, dashed-lines and $f = 20\,\mathrm{pC/m}$, dotted-lines) on the nonlinear static deflection of the CPNB: ($V_0 = 500$ v)

After confirming the current results some case studies are addressed here.

Table 2 The current first two linear natural frequencies in comparison with those of Arvin (2018) (MHz)

Frequency	Results of Arvin (2018)	Current results	Difference percent
ω_1	0.3108	0.3107	0.03
ω_2	1.9326	1.9468	0.73

4.1 Case studies: static deflection

The nonlinear static deflection of the given CPNB which undergoes different applied voltages is depicted in Fig. 3. It can be seen that the static deflection is increased by increment in the applied voltage magnitude.

Figure 4 demonstrates the nonlinear static deflection of the CPNB for different flexoelectric coefficients. As it is expected, according to the last boundary condition in Eq. 23, increment in the flexoelectric magnitude increases the resulting applied moment at the tip point of the beam and subsequently CPNB experiences higher static deflection.

The scale factor influences on the nonlinear static response of the CPNB is investigated in Fig. 5 for an assumed voltage. As it is shown, due to hardening effect of the scale factor on the beam stiffness, the static deflection of the CPNB is decreased by increasing the scale factor.

4.2 Case studies: linear natural frequencies

After the static deflection analysis some case studies for linear natural frequencies are presented here. The length scale parameter and flexoelectric coefficient influences on the first three linear natural frequencies for an assumed constant applied voltage, respectively, are examined in Figs. 6, 7, and 8. The hardening effects of flexoelectric coefficient and the material length scale parameter is obvious. A very interesting phenomenon is evident in the figures. At the beginning, when the flexoelctric constant is small enough, the length scale has a dominant role in stiffness of the considered CPNB while by growing the flexoelectric constant the induced stiffness due to flexoelectricity overcomes the length scale parameter one. The augmented induced stiffness by the increment of the flexoelectric coefficient, is because of the increasing of the static deflection by the increment in the flexoelectric constant which was demonstrated in Fig. 4.

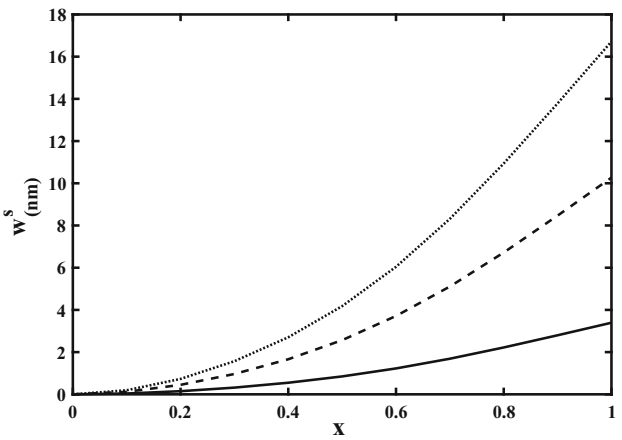

Fig. 5 The effect of the material length scale factor with respect to the beam thickness ratio ($l/h = 0$, dotted-lines, $l/h = 0.2$, dashed-lines and $l/h = 0.5$, solid-lines) on the nonlinear static deflection of the CPNB ($V_0 = 500$ v)

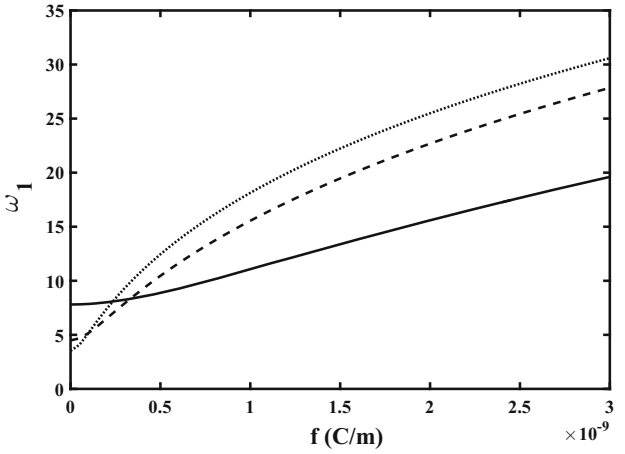

Fig. 6 The effect of the length scale parameter to the beam thickness ratio, i.e. *l*/*h*, on the first natural frequency in terms of the flexoelectric coefficient (dotted-lines, $l/h = 0$, dashed-lines, $l/h = 0.2$ and solid-lines, $l/h = 0.5$) $V_0 = 500$ v

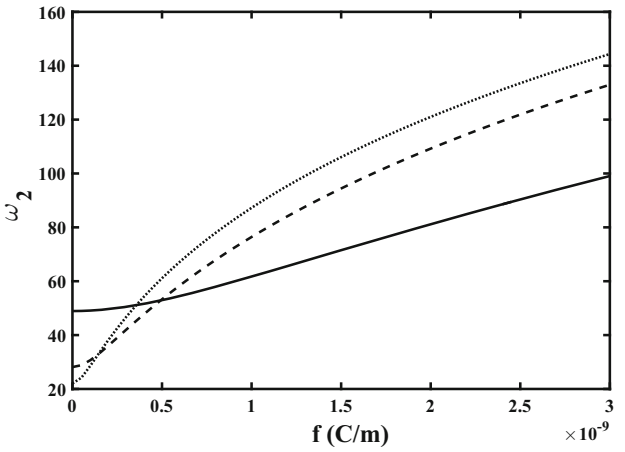

Fig. 7 The effect of the length scale parameter to the beam thickness ratio, i.e. *l*/*h*, on the second natural frequency in terms of the flexoelectric coefficient (dotted-lines, $l/h = 0$, dashed-lines, $l/h = 0.2$ and solid-lines, $l/h = 0.5$) $V_0 = 500$ v

The variation of the first natural frequency with respect to the applied voltage for different flexoelectric coefficient is demonstrated in Fig. 9. It can be inferred that by increasing the applied voltage, the flexoelectric constant plays more significant role in the structural stiffness and makes the CPNB stiffer.

4.3 Case studies: nonlinear free vibration analysis

Here some case studies are examined on the nonlinear free vibration features of the CPNB. The effective nonlinearity

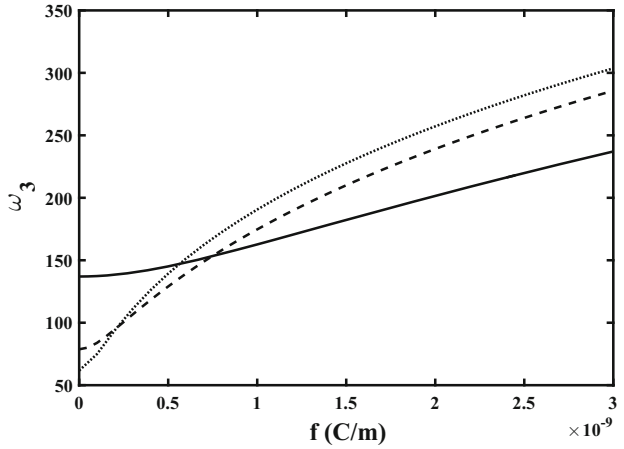

Fig. 8 The effect of the length scale parameter to the beam thickness ratio, i.e. *l*/*h*, on the third natural frequency in terms of the flexoelectric coefficient (dotted-lines, $l/h = 0$, dashed-lines, $l/h = 0.2$ and solid-lines, $l/h = 0.5$) $V_0 = 500$ v

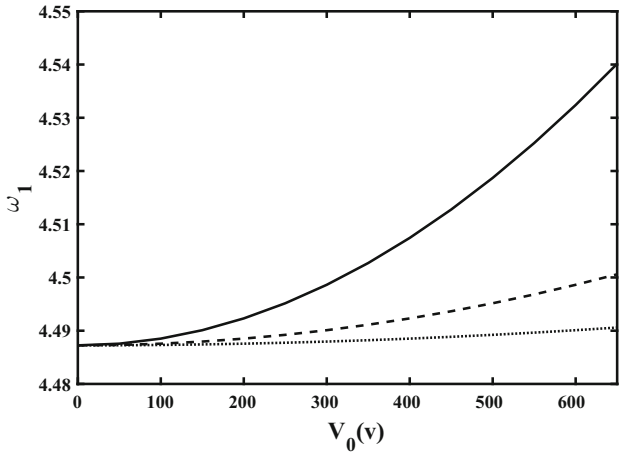

Fig. 9 The effect of the flexoelectric coefficient ($f = 5\,\mathrm{pC/m}$, dotted-lines, $f = 10\,\mathrm{pC/m}$, dashed-lines and $f = 20\,\mathrm{pC/m}$ solid-lines) on the first natural frequency

coefficient with respect to the flexoelectric constant for the first three modes is depicted, respectively, in Figs. 10, 11, and 12. From Fig. 10 it can be inferred although a hardening behaviour is evident when the flexoelectric constant is $f = 0$ but the CPNB shows a softening treatment, too. For verification of the predicted treatment when $f = 0$ one can see McHugh and Dowell (2018). In McHugh and Dowell (2018) it is denoted that when just the geometric nonlinearities are considered, for any cantilever beam which is imposed by the inextensibility condition, the hardening behavior is expected for the first mode. When $f = 0$, it can bee seen that the bigger material length scale parameter has the smaller effective nonlinearity due to hardening effects of the material length scale parameter. The analysis of the figure for $f \neq 0$ shows that the hardening or softening behaviour depends on the mutual

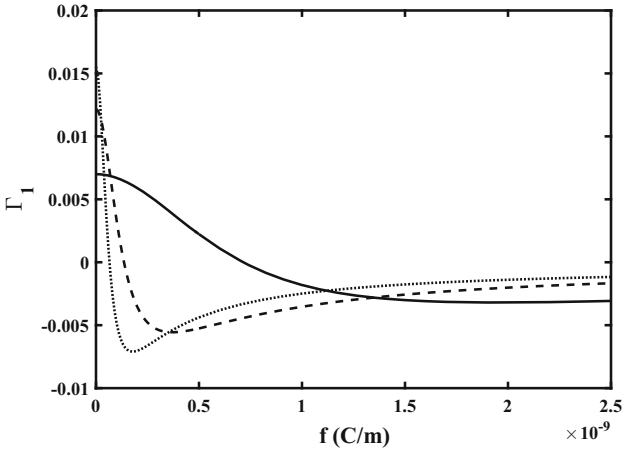

Fig. 10 The effect of the length scale parameter to the beam thickness ratio, i.e. *l*/*h*, on the first mode effective nonlinearity coefficient in terms of the flexoelectric coefficient (dotted-lines, $l/h = 0$, dashed-lines, $l/h = 0.2$ and solid-lines, $l/h = 0.5$)

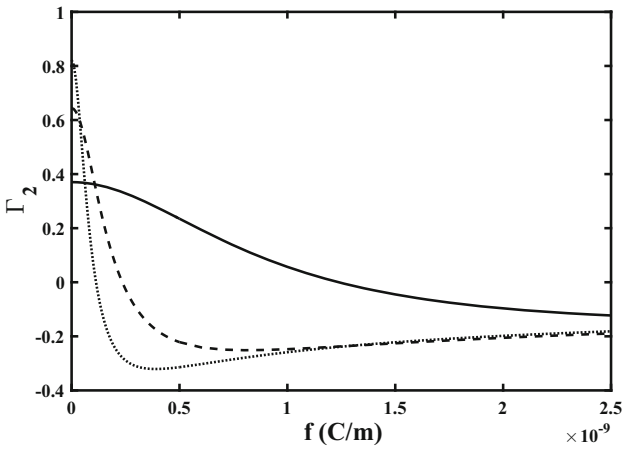

Fig. 11 The effect of the length scale parameter to the beam thickness ratio, i.e. *l*/*h*, on the second mode effective nonlinearity coefficient in terms of the flexoelectric coefficient (dotted-lines, $l/h = 0$, dashed-lines, $l/h = 0.2$ and solid-lines, $l/h = 0.5$)

relation of the material length scale ratio and the flexoelectric constant values and necessarily the CPNB doesn't show the same behaviour for different material length scale parameter at a specified flexoelectric constant or viceversa. Another implication is that by increasing the material length scale parameter the range of the flexoelectric constant which enforces a softening behaviour to the first mode reduces. Also, for all of *l*/*h* ratios, after the CPNB treats as a soften beam in the first mode it will not show again a hardening treatment.

Figure 11 illustrates the second effective nonlinearity coefficient. The hardening behaviour when $f = 0$ is clear which can be proved by McHugh and Dowell (2018). In addition, again when $f = 0$ the material length scale parameter with bigger value takes the smaller effective

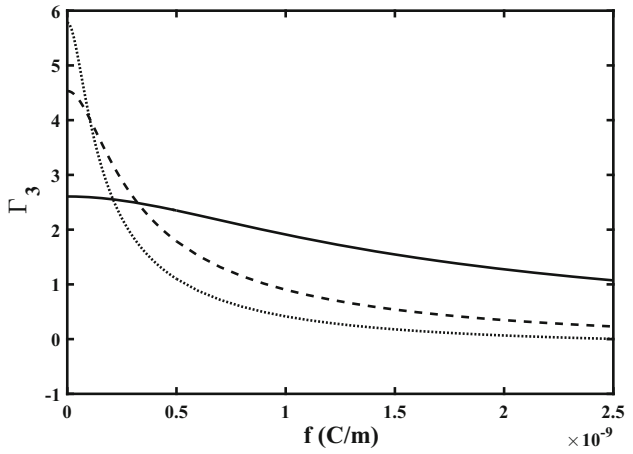

Fig. 12 The effect of the length scale parameter to the beam thickness ratio, i.e. *l*/*h*, on the third mode effective nonlinearity coefficient in terms of the flexoelectric coefficient (dotted-lines, $l/h = 0$, dashed-lines, $l/h = 0.2$ and solid-lines, $l/h = 0.5$)

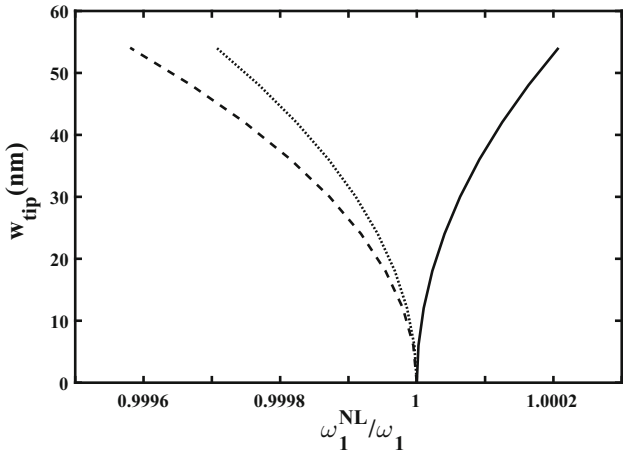

Fig. 14 The effect of the length scale parameter to the beam thickness ratio, i.e. *l*/*h*, on the first frequency ratio in terms of the deflection of the tip point of the CPNB (dotted-lines, $l/h = 0$, dashed-lines, $l/h = 0.2$ and solid-lines, $l/h = 0.5$) for $f = 500\,\mathrm{pC/m}$

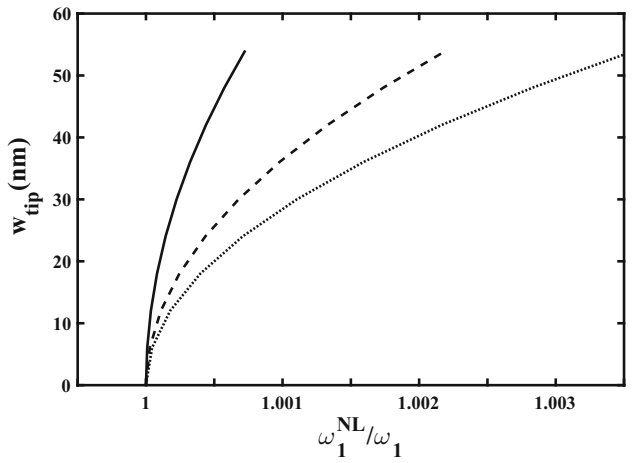

Fig. 13 The effect of the length scale parameter to the beam thickness ratio, i.e. *l*/*h*, on the first frequency ratio in terms of the deflection of the tip point of the CPNB (dotted-lines, $l/h = 0$, dashed-lines, $l/h = 0.2$ and solid-lines, $l/h = 0.5$) for $f = 0\,\mathrm{pC/m}$

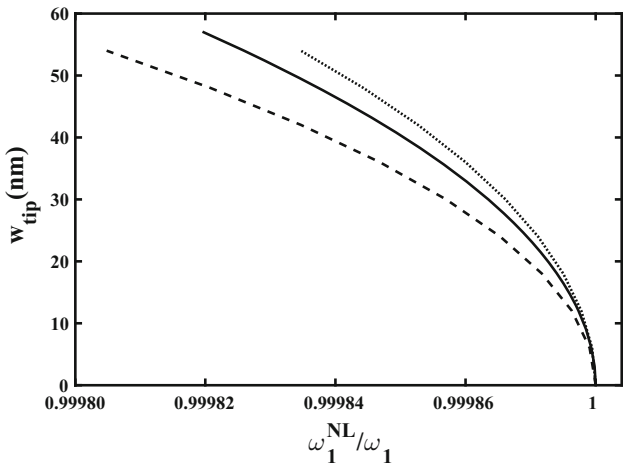

Fig. 15 The effect of the length scale parameter to the beam thickness ratio, i.e. *l*/*h*, on the first frequency ratio in terms of the deflection of the tip point of the CPNB (dotted-lines, $l/h = 0$, dashed-lines, $l/h = 0.2$ and solid-lines, $l/h = 0.5$) for $f = 1000\,\mathrm{pC/m}$

nonlinearity. The figure illustrates for $f \neq 0$ when the hardening treatment shifts to a softening behaviour and the latter behaviour remains for the CPNP. On the other hand, although the starting hardening behaviour for $l/h = 0$ and $l/h = 0.2$ shifts rapidly by increasing the flexoelectric constant to a softening treatment but this sharp negative slope will change into a slow positive slope but never turns into a hardening behaviour.

The effective nonlinearity of third mode is displayed in Fig. 12. A hardening behaviour is predicted for the third mode when the flexoelectric constant is $f = 0$ which can be verified by McHugh and Dowell (2018). In agreement with the first and second modes when $f = 0$ a greater value of the material length scale parameter illustrates a smaller effective nonlinearity. The assessment of the achieved results when $f \neq 0$ demonstrates a monotonous decrement of the effective nonlinearity for all cases by the continuous increment in the flexoelectric constant. The rate of decrement decreases by the increase of the material length scale parameter due to the hardening effects of the material length scale parameter. On the other hand, the figure illustrates that the third mode always represents a hardening mode, in the current range of the flexoelectric constant, independent of the material length scale ratio and the flexoelectric constant.

For more illustrations the nonlinear natural frequency to the corresponding linear natural frequency ratio in terms of the beam tip deflection for the first mode for four different flexoelectric constants are presented in Figs. 13, 14, and 15. These figures in agreement with Fig. 10 demonstrate the

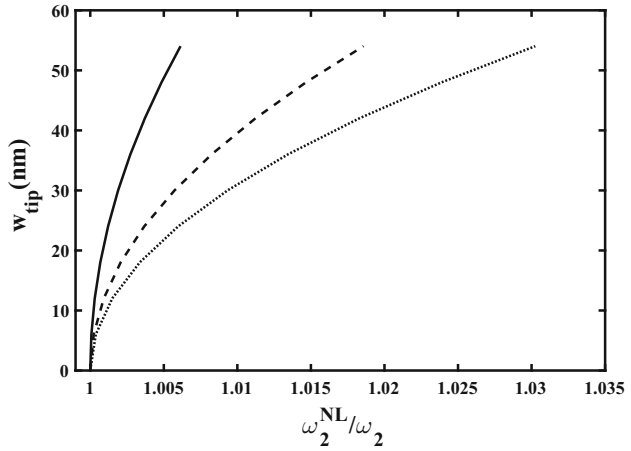

Fig. 16 The effect of the length scale parameter to the beam thickness ratio, i.e. *l*/*h*, on the second frequency ratio in terms of the deflection of the tip point of the CPNB (dotted-lines, $l/h = 0$, dashed-lines, $l/h = 0.2$ and solid-lines, $l/h = 0.5$) for $f = 0\,\mathrm{pC/m}$

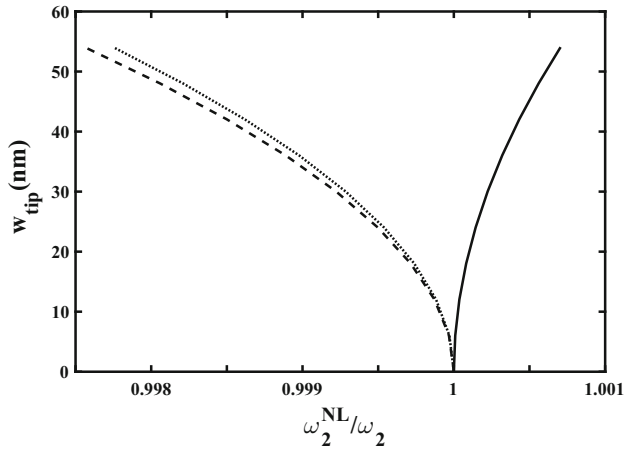

Fig. 17 The effect of the length scale parameter to the beam thickness ratio, i.e. *l*/*h*, on the second frequency ratio in terms of the deflection of the tip point of the CPNB (dotted-lines, $l/h = 0$, dashed-lines, $l/h = 0.2$ and solid-lines, $l/h = 0.5$) for $f = 1000\,\mathrm{pC/m}$

different type of hardening or softening behaviour for the first mode which is tightly related to the material length scale parameter and the flexoelectric coefficient values at the same time.

The second mode nonlinear natural frequency to the associated linear natural frequency ration in terms of the tip deflection of the beam for $f = 0$ pC/m and $f = 1000$ pC/m are depicted, respectively, in Figs. 16 and 17. In accompanied by Fig. 11 the hardening or softening behaviour is predicted for different values of the material length scale parameter and the flexoelectric coefficient.

The similar study as the second mode is performed for the third mode for $f = 0$ pC/m and $f = 1000$ pC/m, respectively, in Figs. 18 and 19. The achieved outcomes are in accordance with Fig. 12.

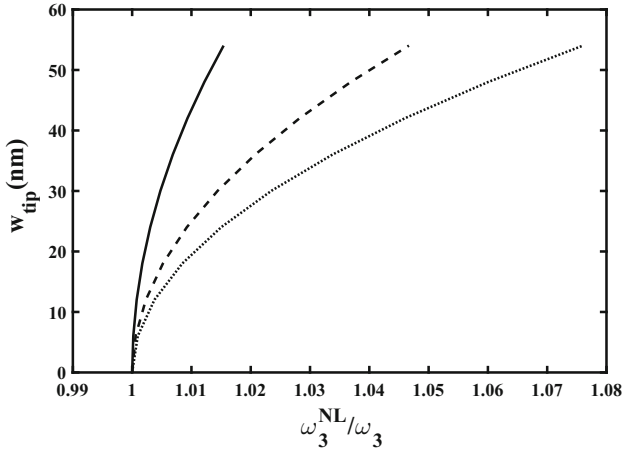

Fig. 18 The effect of the length scale parameter to the beam thickness ratio, i.e. *l*/*h*, on the third frequency ratio in terms of the deflection of the tip point of the CPNB (dotted-lines, $l/h = 0$, dashed-lines, $l/h = 0.2$ and solid-lines, $l/h = 0.5$) for $f = 0\,\mathrm{pC/m}$

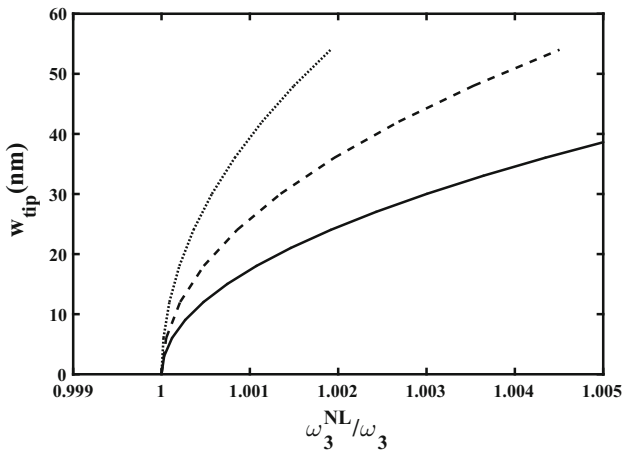

Fig. 19 The effect of the length scale parameter to the beam thickness ratio, i.e. *l*/*h*, on the third frequency ratio in terms of the deflection of the tip point of the CPNB (dotted-lines, $l/h = 0$, dashed-lines, $l/h = 0.2$ and solid-lines, $l/h = 0.5$) for $f = 1000\,\mathrm{pC/m}$

5 Conclusions

The nonlinear free vibration analysis of a pre-actuated nano-cantilever isotropic beam was examined. The formulation was developed for an Euler-Bernoulli inextensible flexoelectric cantilever nanobeam on the basis of the size-dependent flexoelectricity theory. A higher order curvature displacement relation was employed to derive the nonlinear equations of motion by the implementation of the Hamilton's principle. The Galerkin projection approach was applied on the governing partial differential equations of motion to achieve the reduced order equation of motion. The Galerkin approach was implemented to extract the nonlinear static solution due to the pre-applied voltage and the linear natural frequency. The Lindstedt-Poincare

technique was employed to find the nonlinear effective coefficient and the corresponding nonlinear natural frequency. The effects of the applied voltage, the material length scale parameter, and the flexoelectric coefficient on the nonlinear static defection, the linear natural frequency and the nonlinear effective coefficient and the associated nonlinear natural frequency were investigated. The main findings are as follows:

(1) The material length scale parameter and the flexoelectric constant have the hardening effect on the structural stiffness;
(2) Although in the small flexoelectric region, the material length scale parameter effect dominates the flexoelectric influence but with growing the flexoelectric constant it will overcome the material length scale parameter role in the stiffening of the structural stiffness;
(3) When the flexoelectric effect is ignored the inextensible nano-cantilever beam shows a hardening behaviour;
(4) The third mode of nano-cantilever beam always displays a hardening behvaiour;
(5) The mutual relation between the flexoelectric coefficient and the material length scale parameter magnitudes enforces the hardening or softening treatment to the first and second modes of the considered nano-cantilever beam.

Appendix 1: Variation of the stored energy

$$
\begin{aligned}
\delta U &= \int_{\mathcal{V}} (\sigma_{11}\delta e_{11} + 2\mu_{12}\delta\kappa_{21} - D_1\delta E_1 - D_3\delta E_3)dV \\
&= \int_0^L EI(w_{,xxxx} + w_{,xx}^3 + 3w_{,x}w_{,xx}w_{,xxx} + \frac{1}{2}w_{,x}^2 w_{,xxxx})\delta w dx \\
&+ \int_0^L EI\left\{(w_{,xxx} + w_{,x}w_{,xx}^2 + \frac{1}{2}w_{,x}^2 w_{,xxx})\frac{1}{2}w_{,x}^2\right\}\delta w dx \\
&+ \int_0^L \left[A_{11}w_{,xx}\right]_{,xx}\delta w dx \\
&\times EI\left(w_{,xx} + \frac{1}{2}w_{,x}^2 w_{,xx} + A_{11}w_{,xx}\right)\delta w_{,x}\Big|_0^L \\
&- EI\left(w_{,xxx} + w_{,x}w_{,xx}^2 + \frac{1}{2}w_{,x}^2 w_{,xxx}\right)\delta w\Big|_0^L \\
&\times EI\left[\left(w_{,xx} + \frac{1}{2}w_{,x}^2 w_{,xx}\right)\frac{1}{2}w_{,x}^2\right]\delta w_{,x}\Big|_0^L \\
&- EI\left(w_{,xxx} + w_{,x}w_{,xx}^2 + \frac{1}{2}w_{,x}^2 w_{,xxx}\right)\frac{1}{2}w_{,x}^2\delta w\Big|_0^L \\
&+ EI\left(w_{,xx}\frac{1}{2}w_{,x}^2 w_{,xx}\right)w_{,x}w_{,xx}\delta w\Big|_0^L \\
&\times EI\left[\left(w_{,xx} + \frac{1}{2}w_{,x}^2 w_{,xx}\right)w_{,x}w_{,xx} - (A_{11}w_{,xx})_{,x}\right]\delta w\Big|_0^L \\
&+ \int_V \left\{\varepsilon(\Phi_{,xx} + \Phi_{,zz}) + 2f_{,z}w_{,xx}\right\}\delta\Phi dV \\
&- \int_{-b/2}^{b/2}\int_{-h/2}^{h/2} \varepsilon\Phi_{,x}\delta\Phi dy dz\Big|_0^L \\
&- \int_{-b/2}^{b/2}\int_0^L (\varepsilon\Phi_{,z} + 2fw_{,x})\delta\Phi dy dx\Big|_{-h/2}^{h/2}
\end{aligned}
\tag{46}
$$

in which $I = \int_{-b/2}^{b/2}\int_{-h/2}^{h/2} z^2 dydz$, $A_{11} = \int_{-b/2}^{b/2}\int_{-h/2}^{h/2} 4\mu l^2 dydz$ and $E_{11} = \int_{-b/2}^{b/2}\int_{-h/2}^{h/2} f(\Phi_{,z})dydz$.

Appendix 2: The employed parameters for discretization of the equation of motion

$$
\begin{aligned}
\xi_{1,k} &= \int_0^1 \psi_k(x)\psi_k''^3(x)dx \\
\xi_{2,k} &= \int_0^1 \psi_k(x)\psi_k'^2(x)\psi_k^{(4)}(x)dx \\
\xi_{3,k} &= \int_0^1 \psi_k(x)\psi_k'(x)\psi_k''(x)\psi_k'''(x)dx \\
\xi_{4,k} &= \int_0^1 \psi_k(x)w^{s'}\psi_k'(x)\xi_i^{(4)}(x)dx \\
\xi_{5,k} &= \int_0^1 \psi_k(x)w^{s'}\psi_k''(x)\psi_k'''(x)dx \\
\xi_{6,k} &= \int_0^1 \psi_k(x)w^{s''}\psi_k'(x)\psi_k'''(x)dx \\
\xi_{7,k} &= \int_0^1 \psi_k(x)w^{s'''}\psi_k'(x)\psi_k''(x)dx \\
\xi_{8,k} &= \int_0^1 \psi_k(x)w^{s''}\psi_k''^2(x)dx \\
\xi_{9,k} &= \int_0^1 \psi_k(x)w^{s(4)}\psi_k'^2(x)dx \\
\xi_{10,k} &= \int_0^1 \psi_k(x)w^{s'}w^{s(4)}\psi_k'(x)dx \\
\xi_{11,k} &= \int_0^1 \psi_k(x)\psi_k^{(4)}(x)dx \\
\xi_{12,k} &= \int_0^1 \psi_k(x)w^{s'}w^{s''}\psi_k'''(x)dx
\end{aligned}
\tag{47}
$$

$$\xi_{13,k} = \int_0^1 \psi_k(x) w^{s'} w^{s'''} \psi_k''(x) dx$$
$$\xi_{14,k} = \int_0^1 \psi_k(x) w^{s''} w^{s'''} \psi_k'(x) dx$$
$$\xi_{15,k} = \int_0^1 \psi_k(x) w^{s'2} \psi_k^{(4)}(x) dx \quad (47)$$
$$\xi_{16,k} = \int_0^1 \psi_k(x) w^{s''2} \psi_k''(x) dx$$

References

Arvin H (2017) Free vibration analysis of micro rotating beams based on the strain gradient theory using the differential transform method: Timoshenko versus Euler-Bernoulli beam models. Eur J Mech A/Solids 65(20):336–348. https://doi.org/10.1177/1077546317736706

Arvin H (2018) The flapwise bending free vibration analysis of micro-rotating timoshenko beams using the differential transform method. J Vib Control 24(20):4868–4884. https://doi.org/10.1177/1077546317736706

Asif Kh, Heung SK, Byeng DY (2017) Modeling and assessment of partially debonded piezoelectric sensor in smart composite laminates. Int J Mech Sci. https://doi.org/10.1016/j.ijmecsci.06.031

Barari A, Kaliji HD, Ghadimi M, Domairry G (2011) Non-linear vibration of Euler-Bernoulli beams. Latin Am J Solids Struct 8:139–148

Barati MR (2017) Investigating nonlinear vibration of closed circuit flexoelectric nanobeams with surface effects via Hamiltonian method. Microsyst Technol. https://doi.org/10.1007/s00542-017-3549-8

Baskaran S, He X, Chen Q, Fu JF (2011) Experimental studies on the direct flexoelectric effect in a phase polyvinylidene fluoride films. Appl Phys Lett 98:242901

Cady WG (1964) Piezoelectricity: an introduction to the theory and applications of electromechanical phenomena in crystals, new rev, ed, vol 2. Dover, New York

Casadei F, Dozio L, Ruzzene M, Cunefare KA (2010) Periodic shunted arrays for the control of noise radiation in an enclosure. J Sound Vib 329:3632–3646

Dohn S, Sandberg R, Svendsen W, Boisen A (2005) Enhanced functionality of cantilever based mass sensors using higher modes. Appl Phys Lett 86(23):233501

Ebrahimi F, Barati MR (2004) Dynamic modeling of embedded nanoplate systems incorporating flexoelectricity and surface effects. Micorsyst Technol. https://doi.org/10.1007/s00542-018-3946-7

Ebrahimi F, Barati MR (2018) Magnetic field effects on buckling characteristics of smart flexoelectrically actuated piezoelectric nanobeams based on nonlocal and surface elasticity theories. Microsyst Technol. https://doi.org/10.1007/s00542-017-3652-x

Ebnali Samani MS, Tadi Beni Y (2018) Size dependent thermo mechanical buckling of the flexoelectric nanobeam. Mater Res Express 5(8):085018. https://doi.org/10.1088/2053-1591/aad2ca

Fei P, Yeh P, Zhou J, Xu S, Gao Y, Song J (2009) Piezoelectric potential gated field-effect transistor based on a free-standing ZnO wire. Nano Lett 9:3435–9

Hadjesfandiari AR (2013) Size-dependent piezoelectricity. Int J Solids Struct 50:2781–2791

Hadjesfandiari AR, Dargush FG (2011) Couple stress theory for solids. Int J Solids Struct 48:2496–2510

Hao Z, Liao B (2010) An analytical study on interfacial dissipation in piezoelectric rectangular block resonators with in-plane longitudinal-mode vibrations. Sens Actuators A Phys 163:401–409

Haq M (2019) Application of piezo transducers in biomedical science for health monitoring and energy harvesting problem. Mater Res Express 6(2):022002. https://doi.org/10.1088/2053-1591/aaefb8

He J, Hsin C, Liu J, Chen L, Wang Z (2007) Piezoelectric gated diode of a single ZnO nanowire. Adv Mater 19:781–4

Kim P, Bae S, Seok J (2012) Resonant behaviors of a nonlinear cantilever beam with tip mass subject to an axial force and electrostatic excitation. Int J Mech Sci 64(1):232–257

Komijani M, Reddy JN, Eslami MR (2014) Nonlinear analysis of microstructure-dependent functionally graded piezoelectric material actuators. J Mech Phys Solids 63:214–227

Maranganti R, Sharma ND, Sharma P (2006) Electromechanical coupling in nonpiezoelectri materials due to nanoscale nonlocal size effects: Green's function solutions and embedded inclusions. Phys Rev B 74:14110-1–14110-14

McHugh K, Dowell E (2018) Nonlinear responses of inextensible cantilever and free-free beams undergoing large deflections. J Appl Mech 85:051008-1-8

Nayfeh SA, Nayfeh AH (1993) Nonlinear interactions between two widely spaced modes-external excitation. Int J Bifurcation Chaos 3(2):417–427

Lacarbonara W (2013) Nonlinear structural mechanics, theory. Dyn Phenom Model. https://doi.org/10.1007/978-1-4419-1276-3

Lavrik NV, Datskos PG (2003) Femtogram mass detection using photothermally actuated nanomechanical resonators. Appl Phys Lett 82(16):2697–2699

Lazarus A, Thomas O, De J-F (2012) Finite element reduced order models for nonlinear vibrations of piezoelectric layered beams with applications to NEMS. Finite Elem Anal Design 49:35–51

Lim CW, Zhen-Qiang Cheng, Reddy JN (2006) Natural frequencies of laminated piezoelectric plates with internal electrodes ZAMM. Z Angew Math Mech 86(5):410–420. https://doi.org/10.1002/zamm,200310254

Park K, Millet LJ, Kim N, Li H, Jin X, Popescu G, Aluru NR, Hsiab KJ, Bashira R (2010) Measurement of adherent cell mass and growth. Proc Natl Acad Sci USA 107(48):20691–20696

Raiteri R, Grattarola M, Butt HJ, Skladal P (2001) Micromechanical cantilever-based biosensors. Sens Actuators B 79(2–3):115–126

Rasekh M, Khadem SE (2011) Pull-in analysis of an electrostatically actuated nano-cantilever beam with nonlinearity in curvature and inertia. Int J Mech Sci 53(2):108–115

Sumali H, Meissner K, Cudney HH (2001) A piezoelectric array for sensing vibration modal coordinates. Sens Actuators A Phys 93:123–131

Tadi Beni Y (2016) Size-dependent electromechanical bending, buckling, and free vibration analysis of functionally graded piezoelectric nanobeams. J Intell Mater Syst Struct 27(16):2199–2215

Tadi Beni Y (2017) A nonlinear electro-mechanical analysis of nanobeams based on the size-dependent piezoelectricity theory. J Mech 33(3):289–301

Tanner S, Gray J, Rogers C, Bertness K, Sanford N (2007) High-Q GaN nanowire resonators and oscillators. Appl Phys Lett 91:203117

Wang G-F, Yu S-W, Feng X-Q (2004) A piezoelectric constitutive theory with rotation gradient effects. Eur J Mech A Solid 23:455–466

Wu G, Datar RH, Hansen KM, Thundat T, Cote RJ, Majumdar A (2001) Bioassay of prostate-specific antigen (PSA) using micro-cantilevers. Nat Biotechnol 19(9):856–860

Yang YT, Callegari C, Feng XL, Ekinci KL, Roukes ML (2011) MEMS mass sensors with uniform sensitivity for monitoring cellular apoptosis, solid-state sensors, actuators and microsystems conference (TRANSDUCERS), Beijing, June 5–9, pp 759–762

Yang LZ, Liangliang Z, Lianying Yu, Minzhong Wang, Yang Gao (2015) An improved displacement boundary condition of piezoelectric cantilever beams ZAMM. Z Angew Math Mech. https://doi.org/10.1002/zamm,201400169

Younis MI, Nayfeh AH (2003) A study of the nonlinear response of a resonant microbeam to an electric actuation. Nonlinear Dyn 31(1):91–117

Zeng S, Wang BL, Wang KF (2017) Static stability analysis of nanoscale piezoelectric shells with flexoelectric effect based on couple stress theory, Microsyst Technol. https://doi.org/10.1007/s00542-018-3734-4